Rewiring regulation on respiro-fermentative metabolism relieved Crabtree effects in Saccharomyces cerevisiae

Synthetic and Systems Biotechnology 7 (2022) 1034–1043

Contents lists available at ScienceDirect

Synthetic and Systems Biotechnology

journal homepage: www.keaipublishing.com/en/journals/synthetic-and-systems-biotechnology

Original Research Article

Rewiring regulation on respiro-fermentative metabolism relieved Crabtree effects in *Saccharomyces cerevisiae*

Yiming Zhang [a,b,1], Mo Su [a,1], Zheng Wang [a], Jens Nielsen [a,c,d], Zihe Liu [a,*]

[a] Beijing Advanced Innovation Center for Soft Matter Science and Engineering, College of Life Science and Technology, Beijing University of Chemical Technology, 100029, Beijing, China
[b] Bloomage Biotechnolgy CO, LTD, 250000, Jinan, China
[c] Department of Biology and Biological Engineering, Chalmers University of Technology, SE2 96, Gothenburg, Sweden
[d] BioInnovation Institute, Ole Maaløes Vej 3, DK2200, Copenhagen N, Denmark

ARTICLE INFO

Keywords:
Respiro-fermentation
Crabtree effect
Saccharomyces cerevisiae
3-Hydroxypropionic acid

ABSTRACT

The respiro-fermentative metabolism in the yeast *Saccharomyces cerevisiae*, also called the Crabtree effect, results in lower energy efficiency and biomass yield which can impact yields of chemicals to be produced using this cell factory. Although it can be engineered to become Crabtree negative, the slow growth and glucose consumption rate limit its industrial application. Here the Crabtree effect in yeast can be alleviated by engineering the transcription factor Mth1 involved in glucose signaling and a subunit of the RNA polymerase II mediator complex Med2. It was found that the mutant with the *MTH1*^{A81D}&*MED2*^{*432Y} allele could grow in glucose rich medium with a specific growth rate of 0.30 h^{-1}, an ethanol yield of 0.10 g g^{-1}, and a biomass yield of 0.21 g g^{-1}, compared with a specific growth rate of 0.40 h^{-1}, an ethanol yield of 0.46 g g^{-1}, and a biomass yield of 0.11 g g^{-1} in the wild-type strain CEN.PK 113-5D. Transcriptome analysis revealed significant downregulation of the glycolytic process, as well as the upregulation of the TCA cycle and the electron transfer chain. Significant expression changes of several reporter transcription factors were also identified, which might explain the higher energy efficiencies in the engineered strain. We further demonstrated the potential of the engineered strain with the production of 3-hydroxypropionic acid at a titer of 2.04 g L^{-1}, *i.e.,* 5.4-fold higher than that of a reference strain, indicating that the alleviated glucose repression could enhance the supply of mitochondrial acetyl-CoA. These results suggested that the engineered strain could be used as an efficient cell factory for mitochondrial production of acetyl-CoA derived chemicals.

1. Introduction

Under glucose rich conditions yeast *Saccharomyces cerevisiae* predominantly consumes glucose via the fermentative pathway, even in the presence of oxygen. In *S. cerevisiae*, the respiration pathway can produce 18 molecules of ATP from 1 molecule of glucose with an estimated P/O ratio of 1.2, while the fermentative pathway can only produce 2 molecules of ATP [1]. The respiro-fermentative metabolism, also referred to as the Crabtree effect, has been studied for decades, in which the carbon flux overflow to fermentation is coupled with the respiration repression. The underlying mechanism involves complex regulatory networks to simultaneously control the fermentation and respiration [2–4]. From an evolutionary perspective, the Crabtree positive yeast seems to favor an increased ATP production rate over the high ATP yield and the 'make-accumulate-consume' strategy seems to benefit survival in natural environments [5–8]. However, the low energy efficiency of respiro-fermentation not only limits biomass production, but also restricts synthesis of non-ethanol chemicals, especially when their synthesis pathways involve higher consumption of energy or redox power than those supplied from fermentation [9]. Previous studies on chemostat cultivations have found that the biomass yield of *S. cerevisiae* can reach up to 0.5 g g^{-1} glucose with a high respiration rate when the dilution rate is below the critical value, normally in the range of 0.2–0.3 h^{-1}. As the dilution rate increases above the value, the respiration rate decreases while fermentation starts to dominate, and the biomass yield decreases [10–12].

Peer review under responsibility of KeAi Communications Co., Ltd.
* Corresponding author.
E-mail address: zihe@mail.buct.edu.cn (Z. Liu).
[1] Equal contribution.

https://doi.org/10.1016/j.synbio.2022.06.004
Received 16 March 2022; Received in revised form 12 June 2022; Accepted 12 June 2022
Available online 15 June 2022

Attempts on pathway engineering have been made to convert *S. cerevisiae* to Crabtree negative in order to achieve high energy efficiency, high biomass yield or product yield, including knocking out hexose transporter genes *(HXT*s), blocking ethanol production pathways, and introducing heterologous acetyl-CoA synthesis pathways, accompanied with adaptive laboratory evolutions (ALEs) [8,13–17]. However, the engineered strains usually grow with specific growth rates below 0.2 h^{-1} and glucose consumption rates below 0.63 g L^{-1} g^{-1} h^{-1}, compared with the wild-type strain with 0.4 h^{-1} and 2.88 g L^{-1} g^{-1} h^{-1}, respectively. The significantly reduced growth and glucose consumption rates limit their industrial application.

ALE studies of pyruvate decarboxylase (pdc) deletion strains have revealed several mutations of regulators that may play important roles in the respiro-fermentative metabolism shift. Studies find *MTH1* mutations can repress the transcription of several hexose transporter genes to reduce the glucose transport, and hereby reduce the metabolic burden from the carbon flux overflow [16,18–21]. Meanwhile, the *MED2*^{*432Y} mutation has been identified with the global regulatory impact for improved cell growth [13]. It is thus interesting to investigate whether their combination can result in synergistic effects to reinforce alleviations of the Crabtree effect while rescue cell growth.

The metabolism shift from fermentation to respiration may direct more carbon flux to the mitochondria and enhance the energy and the mitochondrial acetyl-CoA synthesis, thereof increase production on acetyl-CoA derived products. As an acetyl-CoA derived chemical, 3-hydroxypropionic acid (3-HP) is synthesized from acetyl-CoA by two enzymes acetyl-CoA carboxylase (ACC) and malonyl-CoA reductase (MCR), in which acetyl-CoA is converted to malonyl-CoA by ACC, and then malonyl-CoA is converted to 3-HP by MCR with consumption of NADPH. The enhanced acetyl-CoA supply has been demonstrated to be crucial for 3-HP synthesis in several previous studies [22,23], and thereof it is interesting to investigate whether 3-HP production would be improved with alleviated the Crabtree effect.

Therefore, in this work we studied the effects of *MTH1* and *MED2* alleles in a wild-type strain CEN.PK 113-5D, focusing on fermentation and respiration pathways, as previous studies performed in pdc deletion strains could not reflect their effects on ethanol production. We also performed transcriptome analysis on these engineered mutants to reveal their regulation on cell metabolism. Then we investigated 3-HP production in the mutants by targeting MCR into the yeast mitochondria. This work shed lights for harnessing yeast mitochondria for production of acetyl-CoA derived chemicals.

2. Materials and methods

2.1. Construction of plasmids and yeast strains

Plasmids and strains constructed in this study could be found in Table 1, and primers used in Supplementary Table 1. The yeast CEN.PK 113-5D was used as the reference strain. Genomic engineering of yeast strains was performed using the GTR-CRISPR system according to previous reports [24]. Mutations of *MTH1*^{A81D}, *MTH1*^{I85S}, *MTH1*$^{A81D,\ I85S}$ and *MED2*^{*432Y} were introduced using a 2-step method. First, the spacer sequence (1st spacer) containing the target mutation point was replaced to a 2nd 20 bp spacer sequence using donor DNA with the Cas9 plasmid harboring gRNA targeting 1st spacer. Then the 2nd spacer sequence was replaced using donor DNA and the Cas9 plasmid harboring gRNA targeting 2nd spacer to generate the mutations. The first step of *MTH1* mutation used pCas9_M226 and donor amplified with primers ds226s1 and ds226s1. The second step of *MTH1* mutation used pCas9_M226s and donor amplified with primers ds226_1 and ds226_81(or ds226_85). The first step of *MED2* mutation used pCas9_MED2 and donor amplified with primers med2_s1_1 and med2_s1_2. The second step of *MED2* mutation used pCas9_MED2_N and donor amplified with primers med2_s2_1 and med2_s2_2. The partial deletion mutant of *MTH1* was achieved using pCas9_M226 and donor DNA amplified with ds226_ID1s and ds226_ID2.

Table 1
Plasmids and strains used and constructed in this study.

Plasmid/Strain	Description	Reference
pCas	*2μ, ampR, TEF1p_iCas9I, SNR52p*	[24]
pScURA	*2μ, ampR, gRNA_URA3_SNR52p_tGly*	[24]
pCas9_M226	pCas, *URA3, pSNR52_M81_step1_gRNA_tSNR52*	This study
pCas9_M226s	pCas, *URA3, pSNR52_M81_step2_gRNA_tSNR52*	This study
pCas9_MED2	pCas, *URA3, pSNR52_Med2_step1_gRNA_tSNR52*	This study
pCas9_MED2_N	pCas, *URA3, pSNR52_Med2_step2_gRNA_tSNR52*	This study
pCas9_MTH1p	pCas, *URA3, pSNR52_MTH1p_gRNA_tSNR52*	This study
pUGG1	*ori, AmpR, 2μ, URA3*	[28]
pYC1	*ori, AmpR, 2μ, URA3, pTEF1_CaMCR_tCYC1*	[22]
pMCR1	pUGG1, *pTDH3-CAT2m_CaMCR_tCYC1*	This study
pMCR2	pUGG1, *pPGK1-CAT2m-(MCR-N)-tADH1, pTDH3-CAT2m-(MCR-C)-tCYC1*	This study
CEN.PK 113-5D	*MATa SUC2 MAL8C ura3-52*	[11]
ZS_mth1	CEN.PK 113-5D, *MTH1*^{A81D}	This study
ZS_mth1_2	CEN.PK 113-5D, *MTH1*^{I85S}	This study
ZS_mth1_3	CEN.PK 113-5D, *MTH1*^{A81D,I85S}	This study
ZS_mth1_4	CEN.PK 113-5D, *MTH1-ΔT*	This study
ZS_med2	CEN.PK 113-5D, *MED2*^{*432Y}	This study
ZS_mm	CEN.PK 113-5D, *MTH1*^{A81D}, *MED2*^{*432Y}	This study
MTH1_HXT1p	CEN.PK 113-5D, *MTH1p::HXT1p*	This study
mth1_ HXT1p	ZS_mth1, *MTH1p::HXT1p*	This study
MTH1_PGK1p	CEN.PK 113-5D, *MTH1p::PGK1p*	This study
mth1_PGK1p	ZS_mth1, *MTH1p::PGK1p*	This study
5D_pMCR1	CEN.PK 113-5D, pMCR1	This study
5D_3HP	CEN.PK 113-5D, pMCR2	This study
mm_3HP	ZS_mm, pMCR2	This study

The promoter replacement of *MTH1* was achieved by pCas9_MTH1p and donor DNAs of different promoters.

To harness yeast mitochondria for 3-HP production, the mitochondrial localization sequence (MLS) CAT2m was fused to the N-terminal of CaMCR from *Chloroflexus aurantiacus* [25]. The intact CaMCR and dissected CaMCR with improved activity [26] were cloned into the vector pUGG1 using Golden Gate assembly, resulting in pMCR1 and pMCR2, respectively. In pMCR1, the *pTDH3* fragment amplified with primers P124&P125 harboring *CAT2m* sequence on its 5' tail and the fragment CaMCR-*tCYC1* amplified from pYC1 [22] with primers P126–P128 were assembled [27]. The pMCR-N and pMCR-C were constructed for mitochondrial expression of two dissected parts of CaMCR. In pMCR-N, the fragment *CAT2m_MCR-N* amplified from pMCR1 with P142&P143, *PGK1p* amplified with primers P140&P141 and *ADH1t* with P144&P145 from pYC1 were assembled into pUGG1. In pMCR-C, *TDH3p-CAT2m* amplified with primers P124&P139 and *MCR-C-CYC1t* amplified with P129&P138 from pMCR1 were assembled into pUGG1. pMCR2 was constructed by assembling *pPGK1-CAT2m-(MCR-N)-tADH1*amplified from pMCR-N with P141&P147, and *pTDH3-CAT2M-(MCR-C)* amplified from pMCR-C with P129&P148 into pUGG1.

All enzymes used for PCR and Golden Gates assembly were purchased from New England Biolabs. The kits used for PCR product

purification and plasmid construction were purchased from Omega Bio-Tek.

2.2. Medium and cultivation conditions

LB medium was used for *E. coli* DH5α cultivation, and ampicillin was supplemented to LB medium to a final concentration of 80 mg L^{-1} when needed. YPD medium and SC-URA medium were used for yeast cultivation [28]. All plates contained 15 g L^{-1} agar.

The minimal synthetic medium for yeast fermentation in shake flasks was composed of 5 g L^{-1} $(NH_4)_2SO_4$, 14.4 g L^{-1} KH_2PO_4, 0.5 g L^{-1} $MgSO_4{\cdot}7H_2O$, trace metal solution, vitamin solution, 40 mg L^{-1} uracil and 20 g L^{-1} glucose, with adjusted pH of 6.5. The compositions of trance metal solution and vitamin solution was previously described in Ref. [29]. Yeast cells were precultured in 5 mL YPD medium at 30 °C overnight, then inoculated with an initial OD_{600} of 0.01, and cultured in the 20 mL minimal medium in 250 mL shake flasks at 30 °C. For the mitochondria activity analysis, a mitochondria pyruvate transporter inhibitor UK-5099 (Sigma, USA) dissolved in DMSO was supplemented into medium with a final concentration of 200 nM when OD_{600} reached around 1. The minimal synthetic medium for yeast fermentation in 1L bioreactors (DasGip, Germany) was composed of 5 g L^{-1} $(NH_4)_2SO_4$, 3 g L^{-1} KH_2PO_4, 0.5 g L^{-1} $MgSO_4{\cdot}7H_2O$, 40 mg L^{-1} uracil, 20 g L^{-1} glucose, trace metal solution and vitamin solution, as described in Ref. [30]. For bioreactor batch fermentation, after precultured in shake flasks to exponential phase (OD_{600} ~1), cells were inoculated in bioreactor with an initial OD_{600} of 0.01. The fermentation was performed at 30 °C, with pH controlled at 5 by 2 M KOH and the dissolved oxygen concentration controlled above 30% by adjusting the stirring speed (800–1200 rpm) and the aeration rate (1–1.5 vvm).

All the chemical used for cell cultivations were purchased from Sinopharm Chemical Reagent Corporation, China, if not specifically annotated.

2.3. Measurement of biomass and extracellular metabolites

The biomass was quantified by OD_{600} (optical density at 600 nm) using the spectrophotometer (GENESYS 30 Visible, Thermo Electron Scientific) and cell dry weight (CDW) calculated by the weight of washed cell collected from 5 mL culture. Cells were harvested to a pre-weighed dry microporous filter sheet (Aquo system, 0.22 μm, Φ 50 mm) and washed with sterile water twice using vacuum filtration. Then the sheet with cells folded inside was first dried in the microwave at 100 W for 3 min, and then dried in a glass dryer with allochroic Silica Gel blue for more than 3 days.

Cell samples were centrifuged at 15,000 g for 3 min at 4 °C and the supernatants were then filtered through 0.22 μm polyethersulfone (PES) filters (JIN TENG, China) and collected for extracellular metabolite analysis on a HPLC system (Shimadzu LC-20AT, Japan) with Aminex HPX-87H column (Bio-Rad, USA) with a UV detector and a RID detector at 65 °C. Measurements of glucose, ethanol, pyruvate, succinate, acetate and glycerol were performed as described in Ref. [15]. Measurements of 3-HP were performed using 0.5 mM H_2SO_4 as eluent for 20 min with a flow rate at 0.5 mL min^{-1}. The volume for sample injection was 10 μL.

2.4. Transcriptome analysis

Samples were collected when the OD_{600} reached 0.9–1.2 in triplicate. Around 10 ml broth was transferred into 50 mL falcon tubes with 30 mL crushed ice and centrifuged at 4000 rpm at 4 °C for 3 min. Cell pellets were then quenched in liquid nitrogen immediately and stored at −80 °C before RNA extraction. Total RNA was extracted using TRIzol Reagent (Invitrogen, USA) based on the manufacturer's instructions. The library preparation and sequencing were carried out on the HiSeq instrument (Illumina, USA) by GENEWIZ Inc. Principal Component Analysis (PCA) was plotted according to variance stabilizing normalization and differential gene expression was analyzed according to Benjamini–Hochberg method using the DEseq2 package in the R studio [31]. Reporter Gene Ontology (GO) term analysis was performed using the PIANO (Integrative Analysis of Omics) package in R studio [32]. The functional enrichment analysis of KEGG pathways was performed using the Database for Annotation, Visualization and Integrated Discovery (DAVID) [33].

2.5. Cellular respiration measurement

Cellular respiration was characterized using the oxygen consumption rate (OCR), which can be quantified using Seahorse XFe96 Extracellular Flux Analyzer (Agilent, USA) [34,35]. The OCR assays for cells responding to two different concentrations of glucose, 1 g L^{-1} and 10 g L^{-1}, were performed in six biological replicates. Cells were incubated overnight in YPD medium to exponential growth phase and washed once with sterile water, and diluted by XF base medium (Agilent, USA) with glucose of two different concentrations, including 1 g L^{-1} and 10 g L^{-1} glucose, respectively. Then, 175 μL cell suspensions were transferred into XFe96 microplates with a final concentration of 2×10^5 cells per well. The plates were centrifuged at 500 rpm for 3 min and incubated for 30 min at 30 °C without CO_2, and the OCR measurements were performed at an interval of 6.5 min for three timepoints for basal values. Prior to the assays, the Seahorse sensor cartridges were hydrated overnight and the XFe96 microplates were coated with 25 μL^{-1} poly-L-lysine (25 μg mL^{-1}) for 30 min, and then evaporated to dryness at room temperature.

3. Results

3.1. Effects of the mutations $MTH1^{A81D}$ and $MED2^{*432Y}$ on cell growth and metabolism

Previous studies identified several *MTH1* mutations in glucose sensitive strains, that could relieve the Crabtree effect [15,18–21,36,37]. Among these alleles, $MTH1^{A81D}$, $MTH1^{I85S}$ and *MTH1-ΔT* were investigated as these mutations were positioned in a highly conserved module to form a putative alpha helix [15,21]. The mutagenesis of *MTH1* was performed using the GTR-CRISPR system, generating four mutant strains with $MTH1^{A81D}$, $MTH1^{I85S}$ and *MTH1-ΔT*, respectively. When cultured in minimal medium in shake flasks, growth profiles of the mutants showed that $MTH1^{A81D}$ and *MTH1-ΔT* resulted in reduced cell growth, glucose consumption and ethanol production, while $MTH1^{I85S}$ did not have a significant effect on cell growth compared with the WT strain (Supplementary Fig. 1). The mutants with $MTH1^{A81D}$ and *MTH1-ΔT* accumulated 6 g L^{-1} ethanol within 27 h, and their specific growth rates were both around 0.22 h^{-1}, while the wildtype strain accumulated 8.3 g L^{-1} ethanol within 21 h, with the specific growth rate around 0.38 h^{-1}. Further characterization in bioreactor cultivations revealed that the strain with the $MTH1^{A81D}$ allele consumed glucose slower with less ethanol produced (Fig. 1B), i.e., its specific growth rate decreased by 50%, the biomass yield increased by 36%, and the ethanol yield decreased by 73.9%, compared with the wildtype strain (Fig. 1A).

Next, the mutagenesis of *MED2* was performed in the wild-type strain, generating the mutant strain with $MED2^{*432Y}$ allele. When cultured in minimal medium in bioreactors, the mutant exhibited a slightly higher biomass yield of 0.14 g_{DCW} g_{Glc}^{-1} and specific growth rate of 0.42 h^{-1}, but a lower specific glucose consumption rate of 3.13 g L^{-1} g_{DCW}^{-1} h^{-1} ((Fig. 1C, Table 2), suggesting a higher energy efficiency of cell metabolism.

We thus combined the two alleles, and the strain with $MTH1^{A81D}$&$MED2^{*432Y}$ showed a faster cell growth with the specific growth rate of 0.30 h^{-1} and less ethanol accumulated (Fig. 1D, Table 2). Meanwhile, the biomass yields increased 40% compared with the strain with $MTH1^{A81D}$. Moreover, the strain with $MTH1^{A81D}$&$MED2^{*432Y}$ showed a much shorter ethanol phase (Fig. 1D), which might be resulted

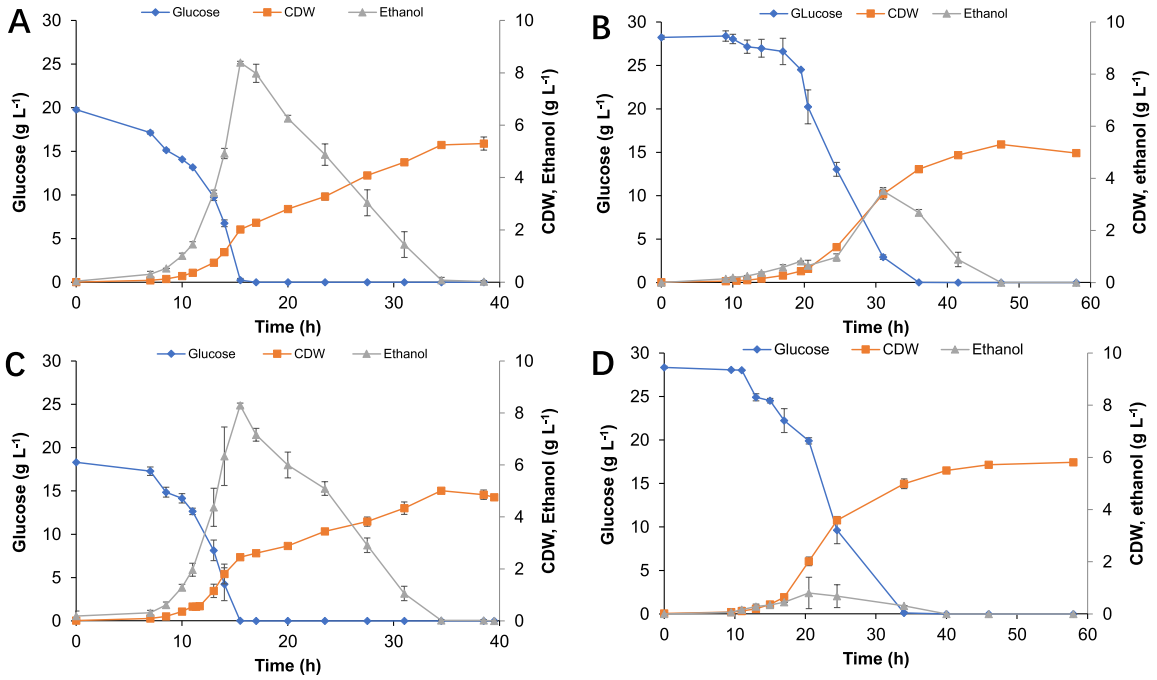

Fig. 1. Growth, glucose and ethanol profiles of the wild-type strain (A) and the mutants with *MTH1* ^{A81D} (B), *MED2*^{*432Y} (C) and *MTH1* ^{A81D}&*MED2*^{*432Y} (D), respectively. The cultivations were performed in minimal medium with 2% glucose in bioreactors in duplicate and error bars represent ±standard errors.

Table 2
Physiological parameters of the wild-type strain (WT) and the mutants with *MED2*^{*432Y} (ZS_med2), *MTH1*^{A81D} (ZS_mth1), and *MTH1*^{A81D}&*MED2*^{*432Y} (ZS_mm), respectively. The cultivations were performed in minimal medium with 2% glucose in bioreactors in replicate. Error bars represent ±standard errors.

	μ_{max}		Y_{SX}		q_{Glu}		Y_{GluEth}		q_{Eth}	
	h^{-1}		$g_{DCW}\ g_{Glc}^{-1}$		$g\ L^{-1}\ g_{DCW}^{-1}\ h^{-1}$		$g_{Eth}\ g_{Glc}^{-1}$		$g\ L^{-1}\ g_{DCW}^{-1}\ h^{-1}$	
WT	0.40	±0.01	0.11	±0.02	3.32	±0.01	0.46	±0.01	1.52	±0.04
ZS_med2	0.42	±0.01	0.14	±0.00	3.13	±0.10	0.45	±0.01	1.39	±0.08
ZS_mth1	0.21	±0.00	0.15	±0.01	1.46	±0.08	0.13	±0.03	0.18	±0.03
ZS_mm	0.30	±0.01	0.21	±0.01	1.47	±0.07	0.10	±0.01	0.15	±0.01

from the altered respiro-fermentative metabolism. Although the strain with *MTH1*^{A81D}&*MED2*^{*432Y} consumed glucose faster than the strain with *MTH1*^{A81D} (Fig. 1B&D), the specific glucose consumption rates of the two strains with *MTH1*^{A81D} and *MTH1*^{A81D}&*MED2*^{*432Y} were almost the same (Table 2), which might be subjected to the restricted glucose uptake rates.

3.2. Transcriptional profiles of the mutant strains

To gain further insights of how the *MED2*^{*432Y} and *MTH1*^{A81D} alleles resulted in altered respiro-fermentative metabolism of the engineered strains, cells of the WT strain and the mutants with *MTH1*^{A81D}, *MED2*^{*432Y} and *MTH1*^{A81D}&*MED2*^{*432Y} were sampled at exponential phase for transcriptome sequencing in triplicate experiments. Principal component analysis of the transcriptome dataset treated with variance stabilizing transformation showed strong reproducibility of biological triplicates (Fig. 2A), and revealed the variances among the strains, which was consistent with the physiological data described above (Table 2).

Differential gene expression analysis (Supplementary Table 2) identified a number of genes with significantly differential expression in the mutants compared with the WT strain (p-adj < 0.01), as shown in Fig. 2B. The *MED2*^{*432Y} allele resulted in 348 genes significantly regulated, while *MTH1*^{A81D} resulted in 3882 genes significantly regulated. The *MED2*^{*432Y}&*MTH1*^{A81D} allele resulted in 3650 genes significantly regulated, in which 3230 genes were shared with those resulted from *MTH1*^{A81D} and 245 genes were identified as commonly differentially expressed among all mutant strains. Gene set enrichment analysis using DAVID bioinformatics resources [33] revealed that 245 commonly differentially regulated genes were significantly enriched in 19 gene sets (p-adj < 0.05) (Fig. 2C), which included glycolytic process, gluconeogenesis, pentose-phosphate shunt, amino acid biosynthesis process, transposition, DNA biosynthetic process, RNA phosphodiester bond hydrolysis, oxidation-reduction process, and transmembrane transport.

Furthermore, reporter GO term analysis using PIANO R package [32] was performed on genes with significantly differential expressions (p-adj < 0.05) for each mutant in comparison with the WT strain (Supplementary Table 3). The mutations of *MED2*^{*432Y}, *MTH1*^{A81D} and *MED2*^{*432Y} &*MTH1*^{A81D} resulted in 25, 176 and 166 GO terms significantly regulated, which suggested different metabolic regulation involving *MED2*^{*432Y} and *MTH1*^{A81D} (Fig. 2D). Top 4 reporter GO terms identified included the downregulated glycolytic process and gluconeogenesis, as well as the upregulated electron transfer chain and heme biosynthesis (Fig. 2E). Meanwhile, other biological processes that were also significantly regulated included amino acid biosynthesis, DNA biosynthetic process, transposition oxidation-reduction process and transmembrane transport (Fig. 2F).

The underlying mechanism for the altered respiro-fermentative metabolism might involve a number of perturbations at the transcriptional level, as well as the post-transcriptional and post-translational

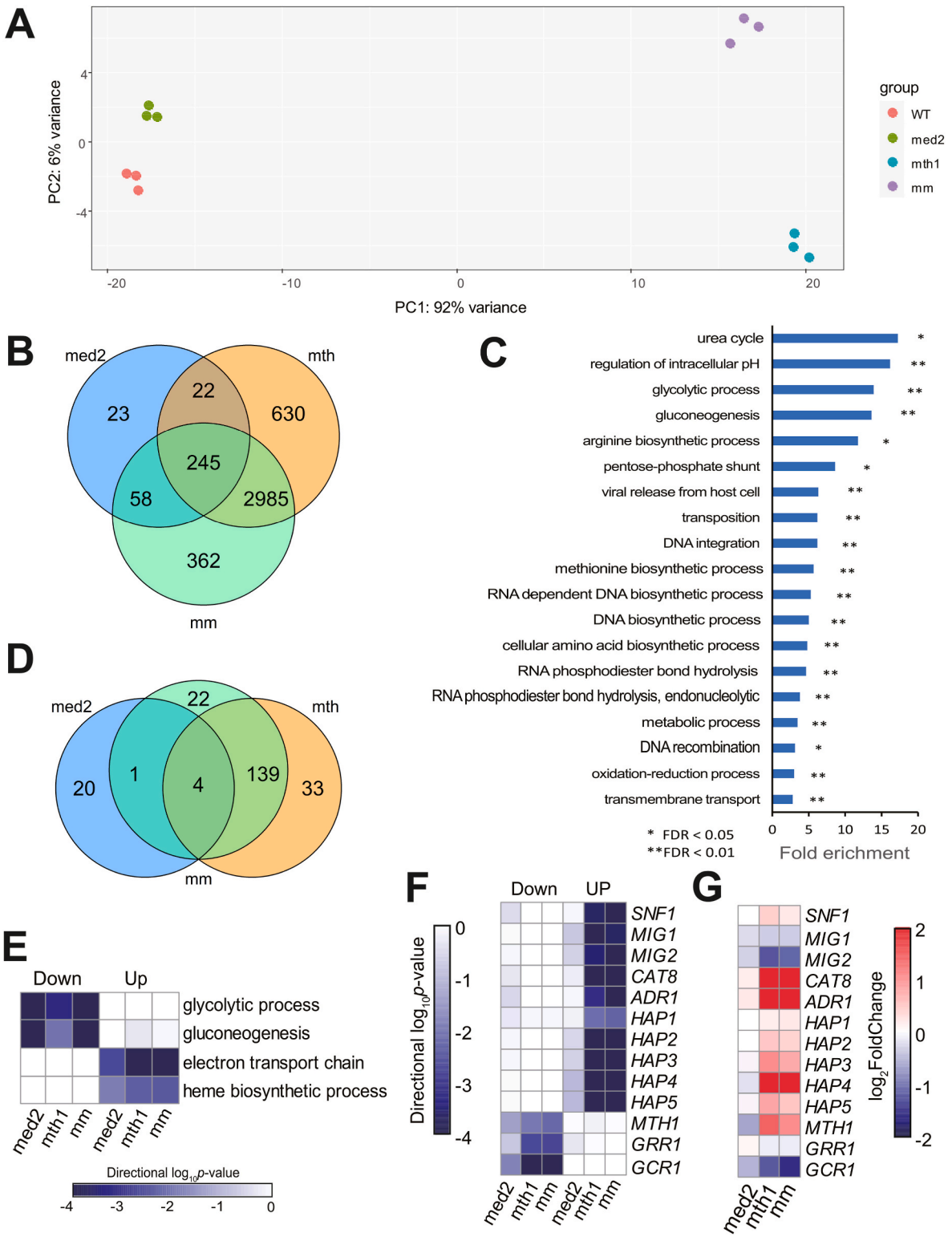

Fig. 2. Transcriptional analysis of the mutant strains. (A) Principal component analysis (PCA) plot of the transcription data in triplicates. (B) Venn diagram of significantly regulated genes of mutant strains in comparison with the WT strain (p-adj < 0.01). (C) Gene set enrichment analysis of the 245 commonly regulated genes. Fold enrichment indicated the magnitude of enrichment against the genome background of the strain S288C analyzed via DAVID. (D) Venn diagram of highly scored (p-value<0.01) reporter GO terms through analyzing significantly regulated genes of the mutants compared with the WT strain (p-adj < 0.05). (E) The common high scored reporter GO terms in distinct-directional up and down class presented by their significance in the mutants. (F) The high scored reporter transcription factors (TFs) in distinct-directional up and down class presented by their significance. (G) Expression levels of reporter TFs in the mutant strains compared with the wildtype strain.

levels. Therefore, we performed reporter TFs analysis, and found several high-scored TFs with their target genes directionally upregulated or downregulated. These reporter TFs and their expression levels were highly relevant for glucose derepression (Fig. 2F&G), including upregulation of *SNF1*, *CAT8*, *ADR1*, *HAP1/2/3/4/5*, and downregulation of *MIG1*, *MIG2*, *MTH1*, *GRR1*, *GCR1*, suggesting the global transcriptional responses resulted from the *MTH1* and *MED2* allele.

3.3. Carbohydrate metabolism and respiration analysis

We further investigated the differentially expressed genes related to carbohydrate metabolism (Fig. 3) and mitochondrial electron transport chains (Fig. 4A). Gene expression levels in the strain with *MED2*^{*432Y} were much more different from those in other two mutants, but more similar with those of strain WT except that the genes related with glycolysis were downregulated, which might support its faster growth as glycolytic enzymes constituted the majority of the cellular proteome [38]. In the two mutants with *MTH1*^{A81D}, most genes related to carbohydrate metabolism were regulated in the same direction but with variations in expression levels, probably due to the global regulation imposed by *MED2*^{*432Y} for a faster growth rate. The major isoforms of hexose transporter encoding genes *HXT1*, *HXT3* and *HXT4* were downregulated, and other glucose transporter genes with high and moderate glucose affinity *HXT6*, *HXT7*, and *HXT10* were upregulated. Most genes of glycolysis, glycerol production, and ethanol production were downregulated, including *PGI1*, *PFK1/2*, *FBA1*, *TDH1/2/3*, *PGK1*, *GPM1*, *ENO1/2*, *CDC19*, *GPD1/2*, *GPP1/2* and *ADH1* et al. Most genes involved in glycogen biosynthesis, glycerol consumption, ethanol consumption, TCA cycle, glyoxylate cycle and fatty acid metabolism were upregulated, which were normally repressed under high glucose conditions (Fig. 3).

The electron transfer chain was coupled with the TCA cycle to completely oxidize acetyl-CoA to CO_2, that consumes oxygen and yields ATP. Reporter GO analysis revealed upregulation of electron transfer chain in all the mutants (Fig. 2E). Therefore, we further investigated differentially expressed genes related to the electron transfer chain in mutant strains, with expression levels presented in Fig. 4A. All genes in the electron cycle were upregulated in the strains with *MTH1*^{A81D}, and around 30% genes were upregulated in the strain with *MED2*^{*432Y}. Moreover, the respiration activities were analyzed through oxygen consumption rate (OCR) measured under two glucose levels, 10 g L^{-1} and 1 g L^{-1}, when the enzymes involved in the TCA cycle and respiration were normally repressed [39]. The mutants showed higher respiration activities compared with the WT strain (Fig. 4B), which was consistent

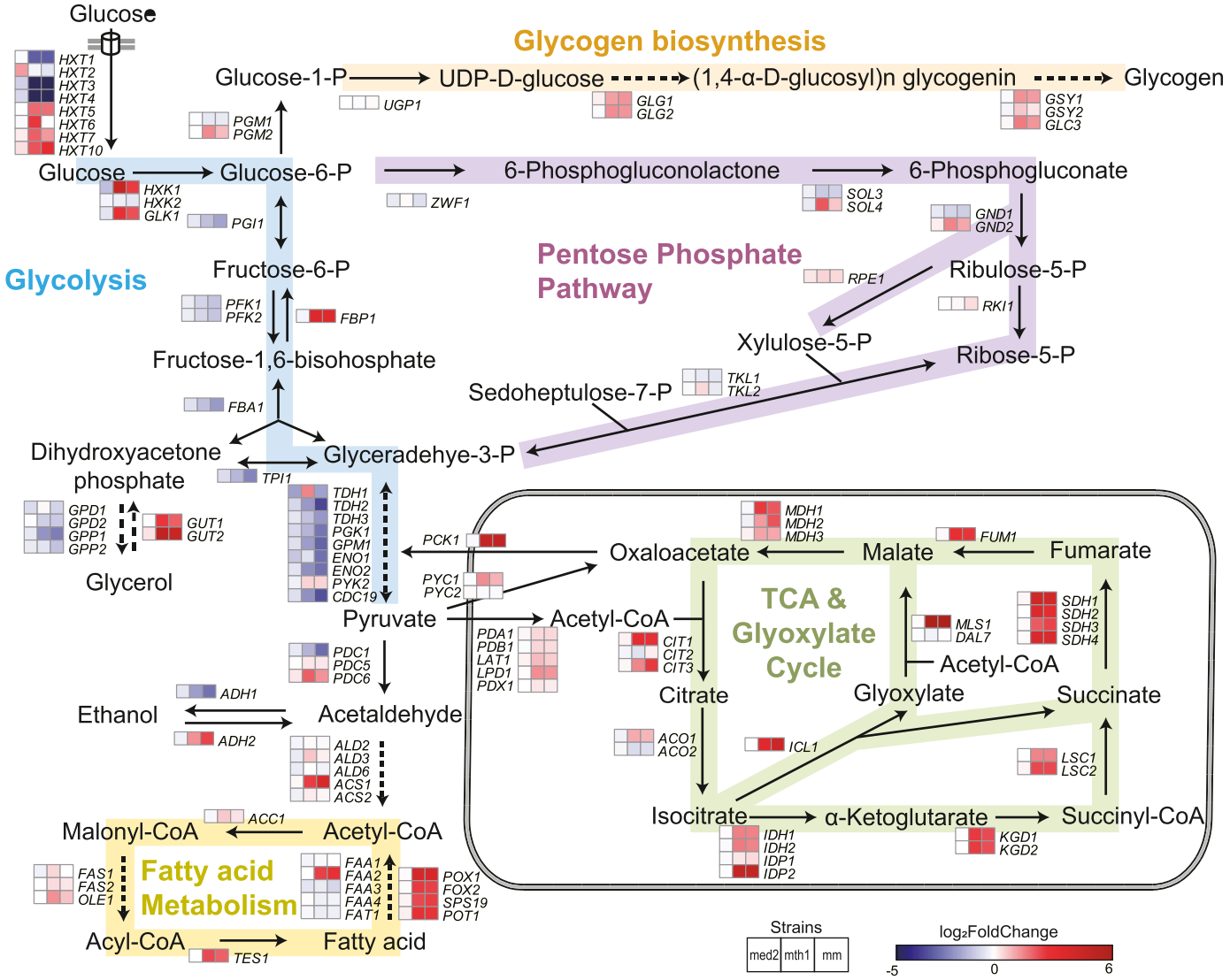

Fig. 3. Transcriptional representation of genes involved in carbohydrate metabolism. All data was made in comparisons with the WT strain.

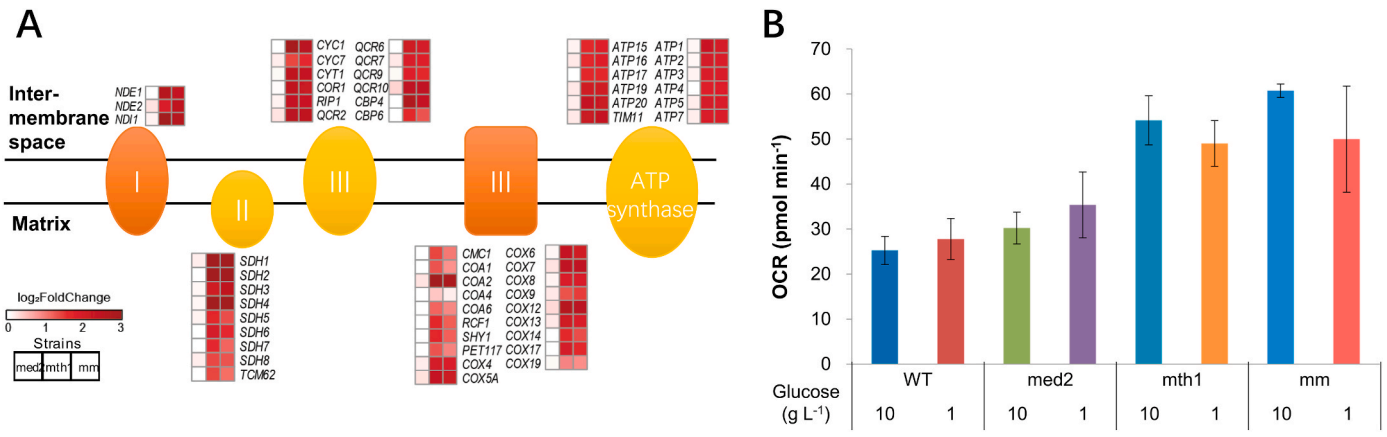

Fig. 4. Effects of *MTH1* and *MED2* mutations on cell respiration. (A) Expression fold changes of the genes involved in mitochondrial electron transport chains. All data were made in comparisons with WT strain. (B) Oxygen consumption rates (OCRs) of the wild-type strain (WT) and mutant strains under two different glucose levels using a Seahorse XF96 analyzer. The measurements were performed in replicate and error bars represent ±standard errors.

with their transcriptional results. The OCR values of the two mutants were about 2-fold higher than those of the WT strain, under both 10 g L^{-1} and 1 g L^{-1} glucose conditions.

Furthermore, to quantify the effects of the elevated mitochondrial activities on cell metabolism, a mitochondrial pyruvate transporter inhibitor UK-5099 was supplemented in the early exponential growth (OD_{600} around 1.0), as inhibited pyruvate transport would thereof restrict the following TCA cycle and electron transport chain. In WT strain and the mutant with *MED2*^{*432Y}, UK-5099 slowed down the growth and ethanol consumption during the ethanol phase (Fig. 5A&C). In the strains with *MTH1*^{A81D}, UK-5099 slowed down the glucose consumption and ethanol accumulation during the glucose phase, as well as growth and ethanol consumption during the ethanol phase (Fig. 5B&D). The results suggested that the respiration pathway subjected to mitochondrial pyruvate transport was derepressed earlier in the strains with *MTH1*^{A81D}, indicating that the TCA cycle and electron transfer chain were derepressed at relatively high glucose.

3.4. Improved 3-HP production in strain ZS_mm with alleviated respiro-fermentative metabolism

The higher enzymatic activities of the TCA cycle and electron transfer chain in the strain with *MED2*^{*432Y} &*MTH1*^{A81D} would probably enhance the mitochondrial acetyl-CoA supply, and thereof improve synthesis of its derived chemicals [22,23]. Therefore, we investigated 3-HP production by expressing CaMCR (MCR from *C. aurantiacus*) in the mitochondria, as mitochondrial acetyl-CoA could be converted to malonyl-CoA by a mitochondrial acetyl-CoA carboxylase Hfa1 [40].

The mitochondrial localization signal of *CAT2* gene CATm was fused at the N terminals of the intact and dissected CaMCR genes to target them into the mitochondria. The intact and dissected CaMCR with CATm were cloned into the episomal plasmids, yielding pMCR1 and pMCR2, respectively. When the two versions of CaMCR expressed in the mitochondria of the WT strain, the dissected one obtained a 3-HP titer of 0.45 g L^{-1}, while the intact one showed a titer of 0.22 g L^{-1} (Supplementary Fig. 2), suggesting a higher enzymatic activity of the dissected

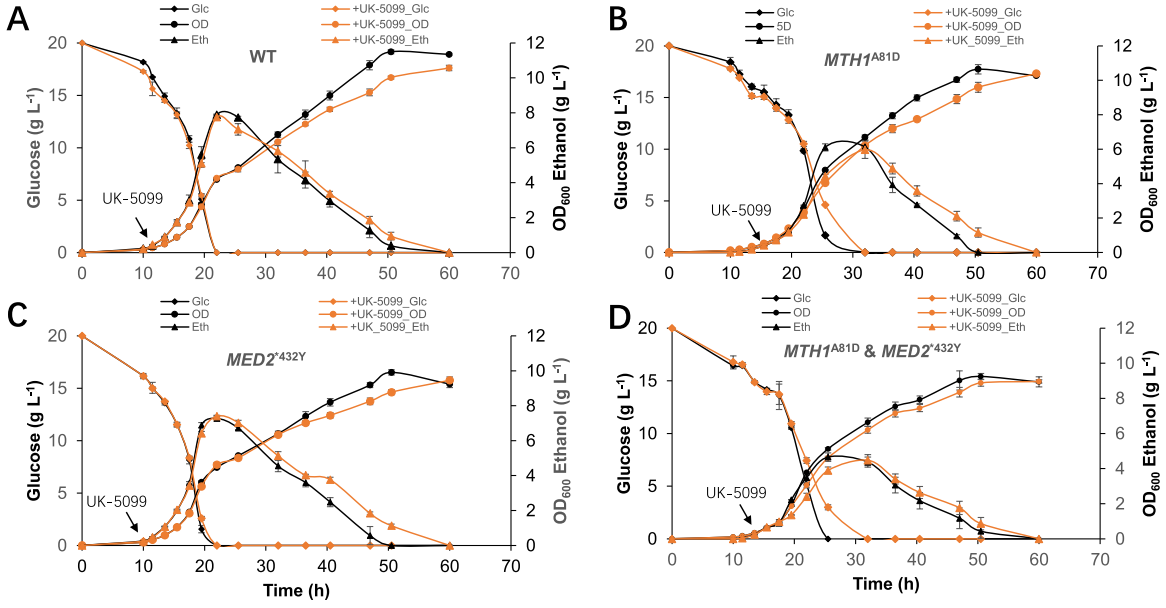

Fig. 5. The growth, glucose and ethanol profiles of the wild-type strain (A) and the mutants ZS_mth1(B), ZS_med2 (C) and ZS_mm (D) with (red line) and without (black line) mitochondrial pyruvate transporter inhibitor UK-5099. The cultivations were performed in minimal medium with 2% glucose in shake flasks in triplicate and error bars represent ±standard errors.

CaMCR.

Then the dissected CaMCR was used for further investigation in the strains of WT and ZS_mm. Briefly, plasmid pMCR2 was transformed into the two strains, generating the strains 5D_3HP and mm_3HP, respectively. The constructed strains were first evaluated for respiration capacity by cultivations –OCR values than those of the 5D_3HP strain under both conditions (Supplementary Fig. 3), confirming its higher respiration activities. Then the strains were evaluated in the minimal medium with 20 g L^{-1} glucose for 3-HP production. As shown in Fig. 6A, the strain 5D_3HP produced 0.35 g L^{-1} 3HP, and more than 75% of 3-HP were accumulated in ethanol phase, as mitochondrial acetyl-CoA supply was restricted due to glucose repression. In the mm_3HP strain, 3-HP accumulated much earlier, and reached to 1.69 g L^{-1} when glucose exhausted, comprising almost 83% of 3-HP titer. The final 3-HP reached as high as 2.04 g L^{-1} at 60 h. These results suggested that the altered respiro-fermentative metabolism of ZS_mm not only could provide higher energy efficiency for biomass formation, and support efficient 3-HP synthesis in the mitochondria, which might be resulted from the derepressed TCA cycle and electron transfer chain.

4. Discussions

Previous studies showed that *MTH1* alleles could improve growth of pdc deletion strains by limiting the glycolysis flux by reducing its degradation [15,16,21], indicating the possibility to regulate glucose uptake rates by manipulating *MTH1* expression levels. Based on FPKM (fragments per kilobase million) values from transcription data (Supplementary Fig. 4), *HXT1p* and *PGK1p* were selected as weaker and stronger promoters compared with *MTH1p*, respectively. Indeed, the strain with reduced Mth1 expression exhibited a fast cell growth, glucose consumption and ethanol accumulation, to similar levels as in the wild-type strain, while the strain with elevated Mth1 expression resulted in a much slower growth, glucose consumption and ethanol accumulation (Supplementary Fig. 5). Yet, the reduced specific growth and glucose uptake rate would hinder its application for production of non-ethanol biochemicals.

The *MED2*^{*432Y} allele was previously reported to improve cell growth of pdc deletion strain by its global regulation on carbon metabolism in pdc deletion strain [13], and in this study it could also improve cell growth of the wild-type and the mutant with *MTH1*^{A81D} allele, which might mainly result from regulation on glycolysis and glucose repression as revealed in our transcriptional analysis. A previous study revealed that glucose transport could impose high control on the glycolytic flux if the capacity reduced below 56% of the wild-type strain [17], which was consistent with our results in which the specific glucose consumption rate of the stain with *MED2*^{*432Y} &*MTH1*^{A81D} was 43.7% of the WT strain. The lower specific ethanol production rate in the strain with *MTH1*^{A81D}&*MED2*^{*432Y} suggested less carbon flux overflow into fermentation and possibly more carbon flux into respiration, and thereof improved cell growth.

The transcription results also revealed the reduced overflow flux to fermentation, and triggered upregulation of the TCA cycle and electron transfer chain. It was noteworthy that several high scored reporter TFs were involved in glucose derepression. Specially, Mig1 and Mig2 functioned as repressors with Snf1 [41–43], while Cat8 and Adr1 functioned as Snf1 activators in glucose derepression associated with gluconeogenesis, glycerol utilization, ethanol utilization, fatty acid utilization and glyoxylate cycle [44–47]. Thus, significant downregulation of *MIG1* and *MIG2* and upregulation of *CAT8* and *ADR1* might result in the glucose derepression. Similarly, upregulation of *HAP1/2/3/4/5*, as transcription activators for respiratory genes [48], could increase mitochondrial biogenesis and the respiratory capacity [49,50]. The upregulation of *MTH1* and downregulation of *GRR1*, required for *HXT*s induction, indicated that *HXTs* might be regulated by both intracellular and extracellular glucose availability. Downregulation of *GCR1*, as an activator of glycolysis genes [51–53], was highly related with significantly downregulation of genes involved in glycolysis process. Deep mining of key players in transcription factors involved in carbohydrate metabolism and respiration could be useful to further improve biomass yield and reduce ethanol yield.

The strain with *MTH1*^{A81D}&*MED2*^{*432Y} could grow with a specific growth rate of 0.30 h^{-1} and specific glucose consumption rate of 1.45 g L^{-1} g_{DCW}^{-1} h^{-1}, which was higher than pdc deletion strains [13,21,26]. Furthermore, the depression of the mitochondrial activities under high glucose levels would make the yeast mitochondria robust compartments for non-ethanol chemical synthesis, as revealed in 3-HP production. The transcriptional results revealed that several genes related to the glyoxylate cycle were also upregulated in the mutant, indicating that peroxisomes could be explored as well. As several studies harnessed yeast mitochondria and peroxisomes for non-ethanol chemical production [56–58], strategies used in this study would be useful to enhanced activities of these compartments. Yet, the specific glucose consumption seemed to be limited by the reduced glucose uptake rate in the strains with the *MTH1*^{A81D} allele. It would be optimal to optimize the glucose uptake rate to increase cell growth while reducing ethanol accumulation for industrial application for non-ethanol production.

5. Conclusions

The *MTH1*^{A81D} and *MED2*^{*432Y} alleles were investigated in wild-type strain for the alleviated Crabtree effects and 3-HP production. The *MTH1*^{A81D} mutation resulted in lower maximum growth rates and ethanol yields accompanied with higher biomass yields. The *MED2*^{*432Y} mutation resulted in improved cell growth rates and biomass yields as

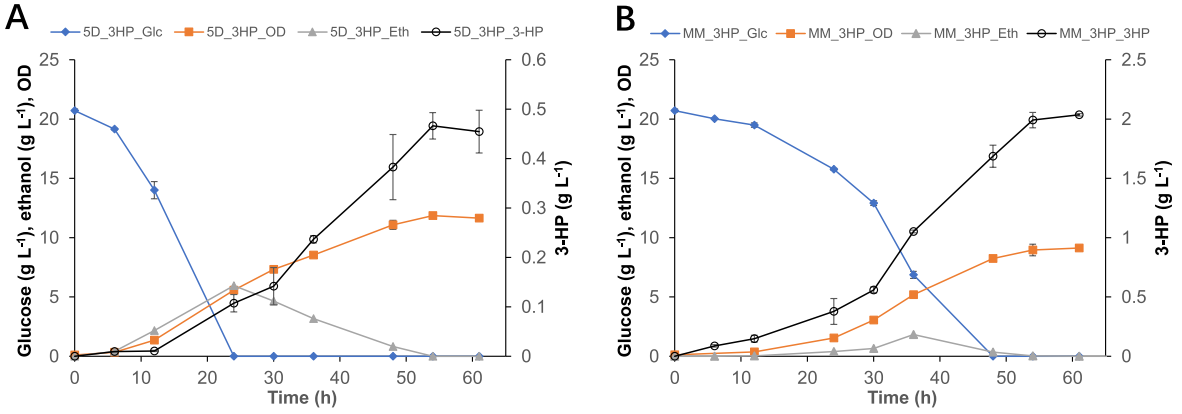

Fig. 6. The growth, glucose, ethanol and 3-HP profiles of the strains without (A) and with (B) the mutations of *MTH1* ^{A81D}&*MED2*^{*432Y}. The cultivations were performed in minimal medium with 2% glucose in shake flasks in triplicate and error bars represent ±standard errors.

well as lower ethanol yields. The transcriptome analysis identified several differentially expressed genes and GO terms, which involved downregulation of glycolytic process and gluconeogenesis and upregulation of electron transfer chain and heme biosynthesis. The strain with *MTH1*^{A81D}&*MED2*^{*432Y} could grow in 2% glucose medium with a specific growth rate of 0.30 h^{-1}, a lower ethanol yield of 0.10 g g^{-1}, and a higher biomass yield of 0.21 g g^{-1}, indicating that the altered carbon flux distribution among fermentation and respiration pathway rendered it a higher energy efficiency. Moreover, with malonyl-CoA reductase expressed in the mitochondria, the engineered strain could produce 3-HP at a titer of 2.04 g L^{-1}, which is 5.4-fold high compared with that of the wild-type strain. The enhance 3-HP production probably benefited from the elevated mitochondrial acetyl-CoA supply resulted from alleviated glucose repression. Therefore, the mutant might be a promising platform strain for mitochondrial synthesis of acetyl-CoA derived chemicals.

Declaration of competing interest

The authors declare no competing interests.

CRediT authorship contribution statement

Yiming Zhang: Conceptualization, Investigation, Formal analysis, Writing – original draft, Writing – review & editing. **Mo Su:** Investigation, Formal analysis, Writing – review & editing. **Zheng Wang:** Investigation, Formal analysis, Writing – review & editing. **Jens Nielsen:** Conceptualization, Supervision, Formal analysis, Writing – review & editing. **Zihe Liu:** Conceptualization, Supervision, Formal analysis, Writing – review & editing.

Acknowledgements

The authors thank for the support from the National Key Research and Development Program of China (2018YFA0900201), National Natural Science Foundation of China (21808008 and 21908004), the Fundamental Research Funds for the Central Universities (buctrc201801), the Beijing Advanced Innovation Center for Soft Matter Science and Engineering, Beijing University of Chemical Technology, and the Knut and Alice Wallenberg Foundation.

Appendix A. Supplementary data

Supplementary data to this article can be found online at https://doi.org/10.1016/j.synbio.2022.06.004.

References

[1] van Gulik WM, Heijnen JJ. A metabolic network stoichiometry analysis of microbial growth and product formation. Biotechnol Bioeng 1995;48(6):681–98. https://doi.org/10.1002/bit.260480617.
[2] Kayikci O, Nielsen J. Glucose repression in *Saccharomyces cerevisiae*. FEMS Yeast Res 2015;15(6). https://doi.org/10.1093/femsyr/fov068.
[3] Gancedo JM. The early steps of glucose signalling in yeast. FEMS Microbiol Rev 2008;32(4):673–704. https://doi.org/10.1111/j.1574-6976.2008.00117.x.
[4] Westergaard SL, Oliveira AP, Bro C, Olsson L, Nielsen J. A systems biology approach to study glucose repression in the yeast *Saccharomyces cerevisiae*. Biotechnol Bioeng 2007;96(1):134–45. https://doi.org/10.1002/bit.21135.
[5] Hagman A, Sall T, Compagno C, Piskur J. Yeast "make-accumulate-consume" life strategy evolved as a multi-step process that predates the whole genome duplication. PLoS One 2013;8(7):e68734. https://doi.org/10.1371/journal.pone.0068734.
[6] Thomson JM, Gaucher EA, Burgan MF, De Kee DW, Li T, Aris JP, Benner SA. Resurrecting ancestral alcohol dehydrogenases from yeast. Nat Genet 2005;37(6):630–5. https://doi.org/10.1038/ng1553.
[7] Pfeiffer T, Morley A. An evolutionary perspective on the Crabtree effect. Front Mol Biosci 2014;1:17. https://doi.org/10.3389/fmolb.2014.00017.
[8] MacLean RC, Gudelj I. Resource competition and social conflict in experimental populations of yeast. Nature 2006;441(7092):498–501. https://doi.org/10.1038/nature04624.
[9] Gambacorta FV, Dietrich JJ, Yan Q, Pfleger BF. Rewiring yeast metabolism to synthesize products beyond ethanol. Curr Opin Chem Biol 2020;59:182–92. https://doi.org/10.1016/j.cbpa.2020.08.005.
[10] van Dijken JP, Bauer J, Brambilla L, Duboc P, Francois JM, Gancedo C, Giuseppin ML, Heijnen JJ, Hoare M, Lange HC, Madden EA, Niederberger P, Nielsen J, Parrou JL, Petit T, Porro D, Reuss M, van Riel N, Rizzi M, Steensma HY, Verrips CT, Vindelov J, Pronk JT. An interlaboratory comparison of physiological and genetic properties of four *Saccharomyces cerevisiae* strains. Enzym Microb Technol 2000;26(9–10):706–14. https://doi.org/10.1016/s0141-0229(00)00162-9.
[11] Canelas AB, Harrison N, Fazio A, Zhang J, Pitkänen J-P, van den Brink J, Bakker BM, Bogner L, Bouwman J, Castrillo JI, Cankorur A, Chumnanpuen P, Daran-Lapujade P, Dikicioglu D, van Eunen K, Ewald JC, Heijnen JJ, Kirdar B, Mattila I, Mensonides FIC, Niebel A, Penttilä M, Pronk JT, Reuss M, Salusjärvi L, Sauer U, Sherman D, Siemann-Herzberg M, Westerhoff H, de Winde J, Petranovic D, Oliver SG, Workman CT, Zamboni N, Nielsen J. Integrated multilaboratory systems biology reveals differences in protein metabolism between two reference yeast strains. Nat Commun 2010;1(1):145. https://doi.org/10.1038/ncomms1150.
[12] Van Hoek P, Van Dijken JP, Pronk JT. Effect of specific growth rate on fermentative capacity of baker's yeast. Appl Environ Microbiol 1998;64(11):4226–33. https://10.1128/AEM.64.11.4226-4233.1998.
[13] Dai Z, Huang M, Chen Y, Siewers V, Nielsen J. Global rewiring of cellular metabolism renders *Saccharomyces cerevisiae* Crabtree negative. Nat Commun 2018;9(1):3059. https://doi.org/10.1038/s41467-018-05409-9.
[14] Otterstedt K, Larsson C, Bill RM, Stahlberg A, Boles E, Hohmann S, Gustafsson L. Switching the mode of metabolism in the yeast *Saccharomyces cerevisiae*. EMBO Rep 2004;5(5):532–7. https://doi.org/10.1038/sj.embor.7400132.
[15] Zhang Y, Liu G, Engqvist MK, Krivoruchko A, Hallstrom BM, Chen Y, Siewers V, Nielsen J. Adaptive mutations in sugar metabolism restore growth on glucose in a pyruvate decarboxylase negative yeast strain. Microb Cell Factories 2015;14:116. https://doi.org/10.1186/s12934-015-0305-6.
[16] van Maris AJ, Geertman JM, Vermeulen A, Groothuizen MK, Winkler AA, Piper MD, van Dijken JP, Pronk JT. Directed evolution of pyruvate decarboxylase-negative *Saccharomyces cerevisiae*, yielding a C2-independent, glucose-tolerant, and pyruvate-hyperproducing yeast. Appl Environ Microbiol 2004;70(1):159–66. https://10.1128/AEM.70.1.159-166.2004.
[17] Elbing K, Larsson C, Bill RM, Albers E, Snoep JL, Boles E, Hohmann S, Gustafsson L. Role of hexose transport in control of glycolytic flux in *Saccharomyces cerevisiae*. Appl Environ Microbiol 2004;70(9):5323–30. https://doi.org/10.1128/AEM.70.9.5323-5330.2004.
[18] Gamo FJ, Lafuente MJ, Gancedo C. The mutation DGT1-1 decreases glucose transport and alleviates carbon catabolite repression in *Saccharomyces cerevisiae*. J Bacteriol 1994;176(24):7423–9. https://doi.org/10.1128/jb.176.24.7423-7429.1994.
[19] Lafuente MJ, Gancedo C, Jauniaux JC, Gancedo JM. Mth1 receives the signal given by the glucose sensors Snf3 and Rgt2 in *Saccharomyces cerevisiae*. Mol Microbiol 2000;35(1):161–72. https://doi.org/10.1046/j.1365-2958.2000.01688.x.
[20] Schulte F, Wieczorke R, Hollenberg CP, Boles E. The HTR1 gene is a dominant negative mutant allele of MTH1 and blocks Snf3-and Rgt2-dependent glucose signaling in yeast. J Bacteriol 2000;182(2):540–2. https://doi.org/10.1128/Jb.182.2.540-542.2000.
[21] Oud B, Flores CL, Gancedo C, Zhang X, Trueheart J, Daran JM, Pronk JT, van Maris AJ. An internal deletion in MTH1 enables growth on glucose of pyruvate-decarboxylase negative, non-fermentative *Saccharomyces cerevisiae*. Microb Cell Factories 2012;11(1):131. https://doi.org/10.1186/1475-2859-11-131.
[22] Chen Y, Bao J, Kim IK, Siewers V, Nielsen J. Coupled incremental precursor and co-factor supply improves 3-hydroxypropionic acid production in *Saccharomyces cerevisiae*. Metab Eng 2014;22:104–9. https://doi.org/10.1016/j.ymben.2014.01.005.
[23] David F, Nielsen J, Siewers V. Flux control at the malonyl-CoA node through hierarchical dynamic pathway regulation in *Saccharomyces cerevisiae*. ACS Synth Biol 2016;5(3):224–33. https://doi.org/10.1021/acssynbio.5b00161.
[24] Zhang Y, Wang J, Wang Z, Zhang Y, Shi S, Nielsen J, Liu Z. A gRNA-tRNA array for CRISPR-Cas9 based rapid multiplexed genome editing in *Saccharomyces cerevisiae*. Nat Commun 2019;10(1):1053. https://doi.org/10.1038/s41467-019-09005-3.
[25] Shi S, Choi YW, Zhao H, Tan MH, Ang EL. Discovery and engineering of a 1-butanol biosensor in Saccharomyces cerevisiae. Bioresour Technol 2017;245(Pt B):1343–51. https://10.1016/j.biortech.2017.06.114.
[26] Liu CS, Ding YM, Zhang RB, Liu HZ, Xian M, Zhao G. Functional balance between enzymes in malonyl-CoA pathway for 3-hydroxypropionate biosynthesis. Metab Eng 2016;34:104–11. https://doi.org/10.1016/j.ymben.2016.01.001.
[27] Engler C, Kandzia R, Marillonnet S. A one pot, one step, precision cloning method with high throughput capability. PLoS One 2008;3(11):e3647. https://doi.org/10.1371/journal.pone.0003647.
[28] Zhang Y, Su M, Qin N, Nielsen J, Liu Z. Expressing a cytosolic pyruvate dehydrogenase complex to increase free fatty acid production in *Saccharomyces cerevisiae*. Microb Cell Factories 2020;19(1):226. https://doi.org/10.1186/s12934-020-01493-z.
[29] Verduyn C, Postma E, Scheffers WA, Vandijken JP. Effect of benzoic acid on metabolic fluxes in yeasts: a continuous-culture study on the regulation of respiration and alcoholic fermentation. Yeast 1992;8(7):501–17. https://doi.org/10.1002/yea.320080703.
[30] Zhang Y, Dai Z, Krivoruchko A, Chen Y, Siewers V, Nielsen J. Functional pyruvate formate lyase pathway expressed with two different electron donors in

Saccharomyces cerevisiae at aerobic growth. FEMS Yeast Res 2015;15(4):fov024. https://doi.org/10.1093/femsyr/fov024.
[31] Love MI, Huber W, Anders S. Moderated estimation of fold change and dispersion for RNA-seq data with DESeq2. Genome Biol 2014;15(12):550. https://doi.org/10.1186/s13059-014-0550-8.
[32] Varemo L, Nielsen J, Nookaew I. Enriching the gene set analysis of genome-wide data by incorporating directionality of gene expression and combining statistical hypotheses and methods. Nucleic Acids Res 2013;41(8):4378–91. https://doi.org/10.1093/nar/gkt111.
[33] Huang da W, Sherman BT, Lempicki RA. Bioinformatics enrichment tools: paths toward the comprehensive functional analysis of large gene lists. Nucleic Acids Res 2009;37(1):1–13. https://doi.org/10.1093/nar/gkn923.
[34] Zhang Y, Lane S, Chen JM, Hammer SK, Luttinger J, Yang L, Jin YS, Avalos JL. Xylose utilization stimulates mitochondrial production of isobutanol and 2-methyl-1-butanol in *Saccharomyces cerevisiae*. Biotechnol Biofuels 2019;12:223. https://doi.org/10.1186/s13068-019-1560-2.
[35] Xu L, Nitika Hasin N, Cuskelly DD, Wolfgeher D, Doyle S, Moynagh P, Perrett S, Jones GW, Truman AW. Rapid deacetylation of yeast Hsp70 mediates the cellular response to heat stress. Sci Rep 2019;9(1):16260. https://doi.org/10.1038/s41598-019-52545-3.
[36] Blazquez MA, Gamo FJ, Gancedo C. A mutation affecting carbon catabolite repression suppresses growth defects in pyruvate carboxylase mutants from *Saccharomyces cerevisiae*. FEBS Lett 1995;377(2):197–200. https://doi.org/10.1016/0014-5793(95)01337-7.
[37] Ozcan S, Freidel K, Leuker A, Ciriacy M. Glucose uptake and catabolite repression in dominant HTR1 mutants of *Saccharomyces cerevisiae*. J Bacteriol 1993;175(17):5520–8. https://doi.org/10.1128/jb.175.17.5520-5528.1993.
[38] Jenjaroenpun P, Wongsurawat T, Pereira R, Patumcharoenpol P, Ussery DW, Nielsen J, Nookaew I. Complete genomic and transcriptional landscape analysis using third-generation sequencing: a case study of *Saccharomyces cerevisiae* CEN.PK113-7D. Nucleic Acids Res 2018;46(7):e38. https://doi.org/10.1093/nar/gky014.
[39] Verduyn C, Zomerdijk TPL, van Dijken JP, Scheffers WA. Continuous measurement of ethanol production by aerobic yeast suspensions with an enzyme electrode. Appl Microbiol Biotechnol 1984;19(3):181–5. https://doi.org/10.1007/BF00256451.
[40] Hoja U, Marthol S, Hofmann J, Stegner S, Schulz R, Meier S, Greiner E, Schweizer E. HFA1 encoding an organelle-specific acetyl-CoA carboxylase controls mitochondrial fatty acid synthesis in *Saccharomyces cerevisiae*. J Biol Chem 2004;279(21):21779–86. https://doi.org/10.1074/jbc.M401071200.
[41] Shashkova S, Wollman AJM, Leake MC, Hohmann S. The yeast Mig1 transcriptional repressor is dephosphorylated by glucose-dependent and -independent mechanisms. FEMS Microbiol Lett 2017;364(14). https://doi.org/10.1093/femsle/fnx133.
[42] Klein CJ, Rasmussen JJ, Ronnow B, Olsson L, Nielsen J. Investigation of the impact of MIG1 and MIG2 on the physiology of *Saccharomyces cerevisiae*. J Biotechnol 1999;68(2–3):197–212. https://doi.org/10.1016/s0168-1656(98)00205-3.
[43] Schmidt GW, Welkenhuysen N, Ye T, Cvijovic M, Hohmann S. Mig1 localization exhibits biphasic behavior which is controlled by both metabolic and regulatory roles of the sugar kinases. Mol Genet Genom 2020;295(6):1489–500. https://doi.org/10.1007/s00438-020-01715-4.
[44] De Vit MJ, Waddle JA, Johnston M. Regulated nuclear translocation of the Mig1 glucose repressor. Mol Biol Cell 1997;8(8):1603–18. https://doi.org/10.1091/mbc.8.8.1603.
[45] Haurie V, Perrot M, Mini T, Jeno P, Sagliocco F, Boucherie H. The transcriptional activator Cat8p provides a major contribution to the reprogramming of carbon metabolism during the diauxic shift in *Saccharomyces cerevisiae*. J Biol Chem 2001;276(1):76–85. https://doi.org/10.1074/jbc.M008752200.
[46] Tachibana C, Yoo JY, Tagne JB, Kacherovsky N, Lee TI, Young ET. Combined global localization analysis and transcriptome data identify genes that are directly coregulated by Adr1 and Cat8. Mol Cell Biol 2005;25(6):2138–46. https://doi.org/10.1128/MCB.25.6.2138-2146.2005.
[47] Young ET, Dombek KM, Tachibana C, Ideker T. Multiple pathways are co-regulated by the protein kinase Snf1 and the transcription factors Adr1 and Cat8. J Biol Chem 2003;278(28):26146–58. https://doi.org/10.1074/jbc.M301981200.
[48] Rosenkrantz M, Kell CS, Pennell EA, Devenish LJ. The Hap2,3,4 transcriptional activator is required for derepression of the yeast citrate synthase gene. Cit1 Mol Microbiol 1994;13(1):119–31. https://doi.org/10.1111/j.1365-2958.1994.tb00407.x.
[49] Bakker BM, Overkamp KM, van Maris AJ, Kotter P, Luttik MA, van Dijken JP, Pronk JT. Stoichiometry and compartmentation of NADH metabolism in *Saccharomyces cerevisiae*. FEMS Microbiol Rev 2001;25(1):15–37. https://doi.org/10.1111/j.1574-6976.2001.tb00570.x.
[50] Lascaris R, Bussemaker HJ, Boorsma A, Piper M, van der Spek H, Grivell L, Blom J. Hap4p overexpression in glucose-grown *Saccharomyces cerevisiae* induces cells to enter a novel metabolic state. Genome Biol 2002;4(1):R3. https://doi.org/10.1186/gb-2002-4-1-r3.
[51] Cha S, Hong CP, Kang HA, Hahn JS. Differential activation mechanisms of two isoforms of Gcr1 transcription factor generated from spliced and un-spliced transcripts in *Saccharomyces cerevisiae*. Nucleic Acids Res 2021;49(2):745–59. https://doi.org/10.1093/nar/gkaa1221.
[52] Baker HV. GCR1 of *Saccharomyces cerevisiae* encodes a DNA binding protein whose binding is abolished by mutations in the CTTCC sequence motif. Proc Natl Acad Sci U S A 1991;88(21):9443–7. https://doi.org/10.1073/pnas.88.21.9443.
[53] Chambers A, Packham EA, Graham IR. Control of glycolytic gene expression in the budding yeast (*Saccharomyces cerevisiae*). Curr Genet 1995;29(1):1–9. https://doi.org/10.1007/BF00313187.